Estimation of the Hindered Settling Function $R(\phi)$ from Batch-Settling Tests

Daniel R. Lester, Shane P. Usher and Peter J. Scales
Particulate Fluids Processing Centre, Dept. of Chemical and Biomolecular Engineering,
The University of Melbourne, Victoria 3010, Australia

DOI 10.1002/aic.10333
Published online March 8, 2005 in Wiley InterScience (www.interscience.wiley.com).

The hindered settling function $R(\phi)$ is a material function that quantifies the interphase drag of colloidal suspensions for all solids volume fractions ϕ. A method is presented to estimate $R(\phi)$ from batch-settling tests for solids volume fractions between the initial solids volume fraction, ϕ_0, and the solids volume fraction at which the suspension forms a continuously networked structure, ϕ_g, known as the gel point. The method is based on an analytic solution of the associated inverse problem. Techniques are presented to address initialization mechanics observed in such tests as well as experimental noise and discrete data. Analysis of synthetic and experimental data suggests that accurate estimates of $R(\phi)$ are possible in most cases. These results provide scope for characterization of suspension dewaterability from batch-settling tests alone. © 2005 American Institute of Chemical Engineers *AIChE J,* 51: 1158–1168, 2005
Keywords: hindered settling function, R(ϕ)*, batch settling, dewaterability characterization*

Introduction

Since Buscall and White (1987) proposed a unified theory for the dewatering of colloidal suspensions, a major challenge has been characterization of the compressive yield stress $P_y(\phi)$, and hindered settling function $R(\phi)$. Pressure filtration techniques characterize the suspension for ϕ corresponding to $P_y(\phi)$ in the pressure range 5–300 kPa (de Kretser et al., 2001; Green et al., 1996; Landman and Russel, 1993; Landman and White, 1992; Landman et al., 1991, 1999; Usher et al., 2001), although it is also desirable to determine these parameters for more dilute systems. In contrast, batch-settling tests are simple to perform, require no specialized equipment, and involve solids concentrations ranging from very dilute up to ϕ_∞, such that $P_y(\phi_\infty) \approx 1$ kPa. These results are relevant to continuous gravity thickening and tailings dam disposal applications.

Although various investigators (de Kretser et al., 2001; Green, 1997; Pashias, 1997; Tiller and Khatib, 1984; Tiller and Shirato, 1964) have proposed methods to characterize the gel point ϕ_g and compressive yield stress $P_y(\phi)$ from batch-settling tests, estimation of $R(\phi)$ is currently limited to the initial solids concentration ϕ_0 only (Green, 1997). Kynch (1952) proposed a graphical method for estimating $R(\phi)$ for $\phi_0 \leq \phi \leq \phi_g$, although because uniqueness conditions had not been established at this juncture (Bustos et al., 1999), physically correct solutions could not be guaranteed. Because appropriate conditions have since been identified by Auzerais et al. (1988), an analytic method of estimating $R(\phi)$ from batch-settling data is presented in this paper. The accuracy of this method is assessed for both synthetic and experimental data.

Batch settling involves the sedimentation and consolidation of a suspension at uniform initial solids concentration ϕ_0 under gravity in a straight-walled vertical vessel. A typical batch-settling experiment is illustrated in Figure 1, the mechanics of which are described by numerous authors (Bürger and Tory, 2000; Bürger and Wedland, 1998; Buscall and White, 1987; Diplas and Papanicolaou, 1997; França et al., 1999; Howells et al., 1990; Landman and White, 1994). Initially, the solids settle to form a clear layer of supernatant ($\phi = 0$) at the top of the column and, simultaneously, a consolidating bed ($\phi \geq \phi_g$)

Correspondence concerning this article should be addressed to P. J. Scales at peterjs@unimelb.edu.au.

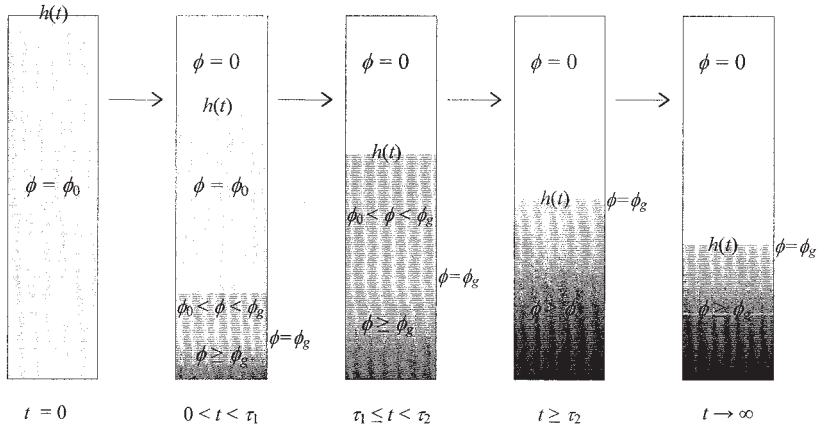

Figure 1. Typical batch-settling experiment.

forms at the base. Depending on the sedimentation type, a transition zone of unnetworked suspension ($\phi_0 < \phi < \phi_g$) can also form between the initial suspension zone ($\phi = \phi_0$) and the consolidating bed. From the start of the test, the initial suspension zone settles until it vanishes at time τ_1, defined as the onset of nonlinear behavior in $h(t)$. The unnetworked transition zone ($\phi_0 < \phi < \phi_g$) continues settling until time τ_2, when only the bed and supernatant remain. The bed may then settle further toward equilibrium, when all of the compressive stress is borne by the solids bed.

The analysis herein facilitates estimation of $R(\phi)$, given the existence of a fan (rarefaction wave) radiating from the origin, which forms part of the transition zone. Another fan with characteristics emanating tangentially from the consolidating bed fills the remainder of this zone. Methods are presented to determine the existence and extent of a fan radiating from the origin, and thus the limits of validity for the analysis.

Batch settling is assumed to be a one-dimensional process and only cases where the suspension is initially unnetworked ($\phi_0 < \phi_g$) are considered here, where both ϕ_0 and ϕ_g are known a priori. Because the network pressure p_N experienced by an element of suspension increases monotonically with time, the condition for irreversible compression ($D\phi/Dt \geq 0$) (Buscall and White, 1987) is automatically satisfied. Therefore the simplification $P_y(\phi) = p_N$ is invoked and so batch settling may be described by the following conservation equation (Bürger and Concha, 1998; Landman and White, 1994)

$$\frac{\partial \phi}{\partial t} + \frac{\partial}{\partial x} f(\phi) - \frac{\partial}{\partial x}\left[D(\phi) \frac{\partial \phi}{\partial x} \right] = 0 \tag{1}$$

subject to the initial and boundary conditions

$$\begin{aligned} &\phi(x, 0) = \phi_0 && 0 \leq x \leq L \\ &\phi(L, t) = 0 && t \geq 0 \\ &\left.\frac{\partial \phi}{\partial x}\right|_{x=0} = \left.\frac{f(\phi)}{D(\phi)}\right|_{x=0} && t \geq 0 \end{aligned} \tag{2}$$

where x is the vertical coordinate, $f(\phi)$ is the settling flux, $D(\phi)$ is the solids diffusion function accounting for sediment compressibility, and L is the initial suspension height. The functions $f(\phi)$ and $D(\phi)$ are given in terms of $P_y(\phi)$ and $R(\phi)$ as

$$f(\phi) \equiv -\frac{(1-\phi)^2}{R(\phi)} \Delta\rho g \phi \tag{3}$$

$$D(\phi) \equiv \begin{cases} 0 & \phi < \phi_g \\ \dfrac{(1-\phi)^2}{R(\phi)} P_y'(\phi) & \phi \geq \phi_g \end{cases} \tag{4}$$

where $\Delta\rho$ is the suspension density difference and g is the gravitational acceleration constant.

Data measurement involves transient recording of the solids/supernatant interface, $h(t)$ (see Figure 1). Because $h(t)$ occurs as a shock in ϕ for monodisperse suspensions, this interface may be detected with accuracy by eye. The challenge of batch-settling analysis is to solve the inverse problem: $h(t) \Rightarrow [R(\phi), P_y(\phi)]$. The nonlinear governing equation (Eq. 1) cannot be solved analytically, and furthermore $h(t)$ is difficult to deconvolute into contributions from each material function. Numeric solution of the inverse problem requires specification of functional forms for $P_y(\phi)$ and $R(\phi)$, may be computationally expensive, and convergence criteria are difficult to determine (Prilepko et al., 2000).

Despite these complications, significant simplifications are possible, given $\phi_0 < \phi_g$. For a series of such batch-settling tests, $P_y(\phi)$ (including ϕ_g) and $R(\phi)$ may be estimated analytically over the ranges $\phi_g \rightarrow \phi_\infty$, $\phi_0 \rightarrow \phi_{\max}$, respectively, where $\phi_{\max}$ represents the maximum analytic estimate of $R(\phi)$ and ϕ_∞ is the maximum ϕ expressed throughout the tests. Subsequently, only $R(\phi)$ in the range $\phi_{\max} \rightarrow \phi_\infty$ need be estimated by numeric solution of the inverse problem; the degrees of freedom are now significantly reduced and convergence can be established.

Transient Batch-Settling Analysis for $\phi < \phi_g$

For $\phi < \phi_g$, $D(\phi)$ is zero by definition, and so Eq. 1 degenerates to the first-order nonlinear equation

$$\frac{\partial \phi}{\partial t} + \frac{\partial}{\partial x} f(\phi) = 0 \tag{5}$$

which can be solved analytically. The time $\tau_{\max}$ is defined as the upper limit of which the dynamics of $h(t)$ may be described by Eq. 5 alone, so this analysis is valid for $t = 0 \rightarrow \tau_{\max}$, and $\phi[h^-(\tau_{\max}), \tau_{\max}] = \phi_{\max}$. Bustos et al. (1999) identify that solutions to Eq. 5 are not unique unless the entropy condition (Oleinik, 1963) is enforced

$$\frac{f(\phi) - f(\phi^-)}{\phi - \phi^-} \leq \sigma(\phi^+, \phi^-) \leq \frac{f(\phi^+) - f(\phi)}{\phi^+ - \phi} \quad \text{for } \phi^- < \phi < \phi^+ \tag{6}$$

where $\sigma(\phi^+, \phi^-)$ is the shock propagation velocity between the two states ϕ^+ and ϕ^-. When applied to gas dynamics, the entropy condition ensures entropy is nonincreasing; however, in the context of sedimentation it relates to conservation of inertia over discontinuities (Auzerais et al., 1988), although inertia is considered negligible otherwise. As a result, different modes of sedimentation arise that are determined by ϕ_0. This analysis is limited to flux curves $f(\phi)$ containing at most one inflection point, as is the case for flux curves corresponding to commonly used functional forms for $R(\phi)$ (de Kretser et al., 2001; Green et al., 1996; Landman et al., 1999; Usher et al., 2001). Such curves give rise to three different sedimentation modes, as characterized by the nature of the $\phi_0 \rightarrow \phi_g$ transition, and Bustos et al. (1999) and Cheng (1981, 1986) analyzed more general forms of $f(\phi)$. Because a fan radiating from the origin is necessary for analytic estimation of $R(\phi)$, settling modes 2 and 3 are divided into the submodes (a) and (b).

- Mode 1: shock
- Mode 2: contact discontinuity: (a) no origin fan, (b) origin fan
- Mode 3: fan: (a) origin fan, (b) no origin fan

If a flux curve does not contain an inflection point ϕ_{inf}, or $\phi_{\text{inf}} \geq \phi_g$, settling mode 1 behavior always results. For $\phi_{\text{inf}} \leq \phi_g$, the settling mode is determined by the value of the initial solids volume fraction ϕ_0 with respect to the concentrations ϕ_1, ϕ_{inf}, $\phi_{\min}$, $\phi_{\max}$

$$\text{Settling mode} = \begin{cases} 0 < \phi \leq \phi_1 & \text{mode 1} \\ \phi_1 < \phi \leq \phi_{\min} & \text{mode 2a} \\ \phi_{\min} < \phi \leq \phi_{\text{inf}} & \text{mode 2b} \\ \phi_{\text{inf}} < \phi \leq \phi_{\max} & \text{mode 3a} \\ \phi_{\max} < \phi < \phi_g & \text{mode 3b} \end{cases} \tag{7}$$

A typical settling flux plot and corresponding critical concentrations are depicted in Figure 2 for an $f(\phi)$ curve with one inflection point. A graphical interpretation of the entropy condition (Eq. 6) is that for any shock, a chord between $[\phi^-, f(\phi^-)]$ and $[\phi^+, f(\phi^+)]$ must lie above the $f(\phi)$ curve. The concentrations ϕ_1 and ϕ_{inf} arise directly from the entropy condition (Eq. 6) and characterize the nature of the lower boundary of the initial suspension zone ($\phi = \phi_0$). For $0 < \phi \leq \phi_1$ a shock forms at this boundary, and for $\phi_{inf} < \phi < \phi_g$ a fan forms. In the region $\phi_1 < \phi \leq \phi_{\text{inf}}$ a fan forms below a contact

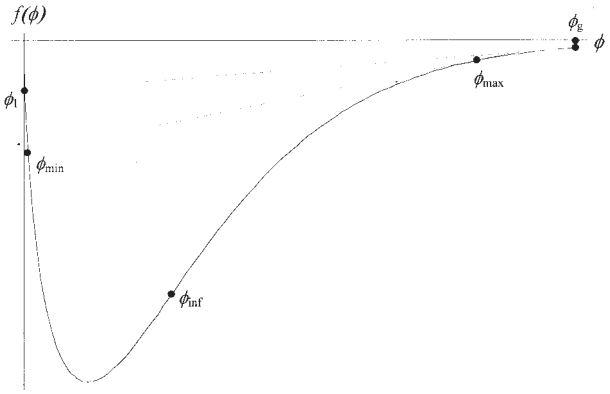

Figure 2. Typical flux plot depicting gel point ϕ_g, analysis limits $\phi_{\min}$, $\phi_{\max}$, inflection point ϕ_{inf}, and mode 1/2 boundary ϕ_1.

discontinuity x_{cd} at the boundary, which has the propagation velocity of both a shock and a characteristic

$$\frac{dx_{cd}}{dt} = \frac{f(\phi^*) - f(\phi_0)}{\phi^* - \phi_0} = f'(\phi^*) \tag{8}$$

where ϕ^* is the solids concentration on the lower side of the contact discontinuity, as determined by Eq. 8. The upper limit for ϕ^* is ϕ_g, and so concentration ϕ_1 corresponds to the lower limit of ϕ_0 for which a contact discontinuity occurs

$$\phi_1 = \phi : f'(\phi_g) = \frac{f'(\phi_g) - f'(\phi)}{\phi_g - \phi} \tag{9}$$

Given $\phi_0 < \phi^*$, the existence of a solution to Eq. 8 requires that $\phi_0 < \phi_{\text{inf}} < \phi^*$, and so ϕ_{inf} represents the upper limit of ϕ_0 for which a contact discontinuity can occur.

The critical concentrations $\phi_{\min}$, $\phi_{\max}$ relate to whether a fan emanating from the origin exists, that is, do characteristics originating from $(x, t) = (0, 0)$ collide with the shock (x_b) corresponding to the consolidating bed? Given that the networked bed is consolidating and is maximal at the origin, it is thus sufficient only to establish whether collision between these characteristics and x_b occurs here. For $\phi \geq \phi_g$, the governing Eq. 1 and the Rankine–Huigonoit condition give the second-order shock dynamics for the consolidating bed as

$$\frac{dx_b}{dt} = \frac{f(\phi^+) - f(\phi^-) + D(\phi^-)\dfrac{\partial \phi^-}{\partial x}}{\phi^+ - \phi^-} \tag{10}$$

where ϕ^+, ϕ^- are the respective solids concentrations above and below the shock; thus $\phi^- = \phi_g$. Because this shock originates from the origin, the boundary condition from Eq. 2 at $x = 0$ yields an expression for the shock velocity at $t = 0$ as

$$\left.\frac{dx_b}{dt}\right|_{t=0} = \lim_{t \rightarrow 0} \frac{f(\phi^+)}{\phi^+ - \phi_g} \tag{11}$$

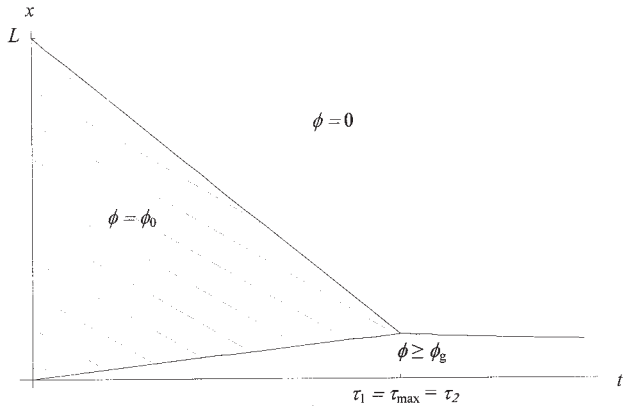

Figure 3. Sedimentation dynamics for settling mode 1.

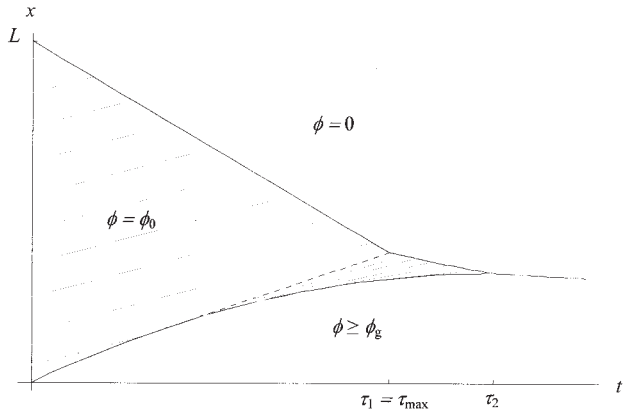

Figure 4. Sedimentation dynamics for settling mode 2a.

Given a fan of characteristics at the origin, the greatest solids volume fraction that can be analyzed is that whose characteristic is tangential to the consolidating bed x_b

$$\phi = \phi^+ : f'(\phi^+) = \frac{f(\phi^+)}{\phi^+ - \phi_g} \tag{12}$$

If $\phi_g > \phi_{inf} - f(\phi_{inf})/f'(\phi_{inf})$, there exist two solutions to Eq. 12, only the upper of which satisfies the entropy condition (Eq. 7). For $\phi_g \leq \phi_{inf} - f(\phi_{inf})/f'(\phi_{inf})$, no solution to Eq. 12 satisfies the entropy condition, so a fan emanating from the origin does not exist. The maximum value of f_0 for which the analysis is valid, ϕ_{max}, is determined as

$$\phi_{max} = \max(\phi) : f'(\phi) = \frac{f(\phi)}{\phi - \phi_g} \quad \text{given } \phi_g > \phi_{inf} - \frac{f(\phi_{inf})}{f(\phi_{inf})} \tag{13}$$

The lower limit of ϕ_0 for valid analysis, ϕ_{min}, arises from the dynamics of the contact discontinuity (Eq. 8). If $\phi^* \geq \phi_{max}$, then no fan emanating from the origin exists because the slope of the contact discontinuity is less than dx_b/dt at the origin. Because ϕ^* decreases with increasing ϕ_0, the analysis is valid for values of $\phi_0 > \phi_{min}$, where ϕ_{min} is such that the corresponding $\phi^* = \phi_{max}$

$$\phi_{min} : f'(\phi_{max}) = \frac{(\phi_{max}) - f(\phi_{min})}{\phi_{max} - \phi_{min}} \tag{14}$$

Because expressions for ϕ_1, ϕ_{min}, and ϕ_{max} have been generated, the conditions (Eq. 7) for each settling mode and submode have been quantified. However, given that $f(\phi)$ is unknown a priori, these modes must be determined solely from the $h(t)$ curve. To do this, the dynamics of each mode is considered and conditions in terms of $h(t)$ derived.

Settling mode 1 is characterized by linear behavior of $h(t)$ up to $t = \tau_1 = \tau_{max}$, as depicted in Figure 3. A shock arises between the sediment and consolidation regions at τ_1, where ϕ steps from ϕ_0 to ϕ_g. In this mode, $h'(t)$ is constant for $t < \tau_1$ and may be discontinuous at $t = \tau_1$.

For settling mode 2a, a transition from linear to nonlinear behavior in $h(t)$ occurs at time $\tau_1 = \tau_{max}$, and here $h'(t)$ is discontinuous, as illustrated in Figure 4. This transition is associated with a contact discontinuity emanating tangentially from the consolidating bed, where ϕ steps from ϕ_0 to ϕ^*. The fan below the contact discontinuity also emanates tangentially from the consolidating bed.

Settling mode 2b differs in that the contact discontinuity (ϕ steps from ϕ_0 to ϕ^*) emanates from the origin, generating a discontinuity in $h'(t)$ at τ_1, as shown in Figure 5. There is fan radiating from the origin, where ϕ increases from ϕ^* to ϕ_{max}, the characteristic of which intercepts the sediment/supernatant interface at τ_{max}. After this, a second fan emanates tangentially from the consolidating bed.

For settling mode 3a, $h(t)$ also changes from linear to nonlinear behavior at τ_1, although in this case $h'(t)$ is continuous, according to Figure 6. The fan radiating from the origin covers the transition from ϕ_0 to ϕ_{max}, and the corresponding characteristics intercept $h(t)$ at τ_1 and τ_{max}, respectively. Again a second fan emanates tangentially from the consolidating bed.

Figure 7 shows mode 3b, where again $h(t)$ is smooth at the transition from linear to nonlinear behavior at $\tau_1 = \tau_{max}$, although now the fan only emanates tangentially from the consolidating bed.

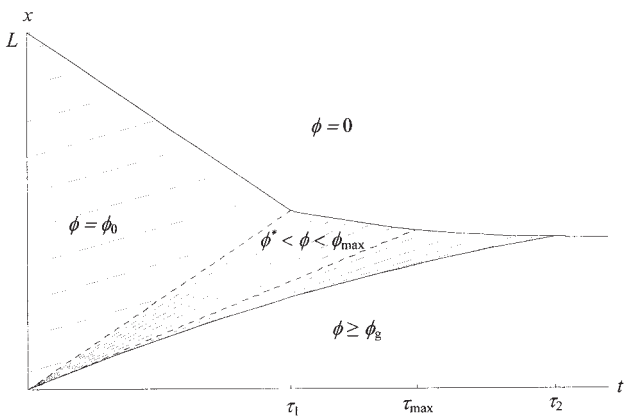

Figure 5. Sedimentation dynamics for settling mode 2b.

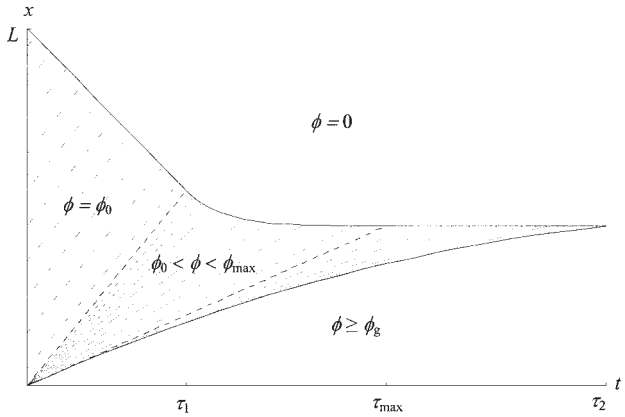

Figure 6. Sedimentation dynamics for settling mode 3a.

Theoretical Analysis of Transient Data

Given that this analysis is valid only for $\phi_{min} < \phi_0 < \phi_{max}$, it is necessary to determine whether ϕ_0 falls in this range from the $h(t)$ curve alone. From analysis of the settling modes, it is clear that ϕ^+ in Eq. 12 may be expressed as

$$\lim_{t\to 0} \phi^+ = \begin{cases} \phi_{max} & \text{if } \phi_g > \phi_{inf} - \dfrac{f(\phi_{inf})}{f'(\phi_{inf})} \quad \text{and} \quad \phi_{min} < \phi_0 < \phi_{max} \\ \phi_0 & \text{otherwise} \end{cases} \tag{15}$$

and so Eq. 12 may be written

$$\left.\frac{dx_b}{dt}\right|_{t=0} \leq -\frac{f(\phi_0)}{\phi_g - \phi_0} \tag{16}$$

Because τ_1 marks the onset of nonlinearity in the $h(t)$ curve, if $h(\tau_1)/\tau_1$ is greater than dx_b/dt at $t = 0$, then a fan radiating from the origin does exist. Thus $\phi_{min} < \phi_0 < \phi_{max}$ corresponds to the condition

$$\frac{h(\tau_1)}{\tau_1} > -\frac{f(\phi_0)}{\phi_g - \phi_0} = -h'(\tau_1^-)\frac{\phi_0}{\phi_g - \phi_0} \tag{17}$$

and so if condition 17 is satisfied, all that remains to be determined is whether submode 2b or submode 3a is present. For mode 2b settling, the contact discontinuity x_{cd} (Eq. 9) intersects $h(t)$ at τ_1

$$\frac{dx_{cd}}{dt} = f'(\phi^*) = \frac{f'(\phi^*) - f'(\phi_0)}{\phi^* - \phi_0} = \frac{h(\tau_1)}{\tau_1} \tag{18}$$

This produces a discontinuity in $h'(t)$ at $t = \tau_1$, the upper limit of which is

$$h'(\tau_1^+) = \frac{f(\phi^*)}{\phi^*} \tag{19}$$

and so ϕ^* may be determined by the jump in $h'(t)$ at τ_1

$$\phi^* = \phi_0 \frac{h(\tau_1) - \tau_1 h'(\tau_1^-)}{h(\tau_1) - \tau_1 h'(\tau_1^+)} \tag{20}$$

It is worth nothing that for mode 3a settling, $h'(t)$ is continuous at $t = \tau_1$, and so Eq. 20 correctly recovers $\phi^* = \phi_0$ in this case. As such, there is no explicit need to distinguish between mode 2b ($\phi^* > \phi_0$) and mode 3a ($\phi^* = \phi_0$) settling in the analysis.

Given satisfaction of condition 17, transformation of the $h(t)$ curve to $f(\phi)$ data is facilitated by considering the dynamics of the characteristics and shocks arising in the various settling modes. Because $h(t)$ always represents a shock, the dynamics of $h(t)$ for $0 \leq t < \tau_{max}$ is given by the Rankine–Hugoniot condition

$$h'(t) = \frac{f(\phi^+) - f(\phi^-)}{\phi^+ - \phi^-} = \frac{f\{\phi^-[h(t), t]\}}{\phi^-[h(t), t]} \tag{21}$$

Also ϕ is constant along the characteristics x_c radiating from the origin, which have the form

$$x_c(t) = f'[\phi(0, 0)]t \tag{22}$$

so these characteristics intercept the $h(t)$ curve at $h(t) = x_c'(t)$, yielding

$$\frac{h(t)}{t} = f'\{\phi^-[h(t), t]\} \tag{23}$$

Therefore the relationship between the settling curve $h(t)$ and flux function $f(\phi)$ for $0 \leq t \leq \tau_{max}$ is given by the symmetric Eqs. 21 and 23

$$h'(t) = \frac{f(\phi)}{\phi} \qquad \frac{h(t)}{t} = f'(\phi) \tag{24}$$

Rewriting $f(\phi)$ as $\phi u(\phi)$, this relationship may be expressed as

$$h'(t) = u \qquad \frac{h(t)}{t} = u + \phi\frac{du}{d\phi} \tag{25}$$

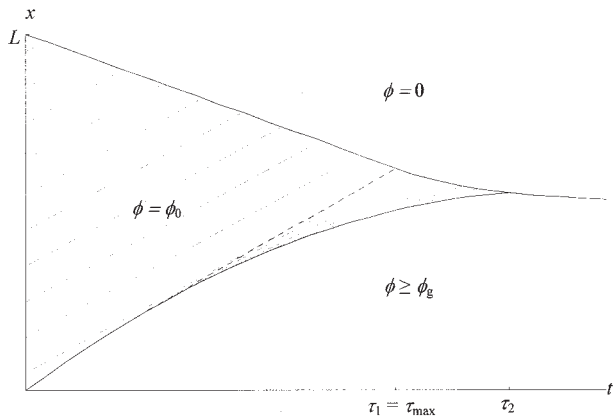

Figure 7. Sedimentation dynamics for settling mode 3b.

Let

$$\xi(t) = \frac{1}{\dfrac{h(t)}{t} - h'(t)} = \frac{1}{\phi}\frac{d\phi}{du} \tag{26}$$

By parameterizing $\xi(t)$ against $h'(t)$, then

$$\xi(t) = \mathcal{J}[h'(t)] \Leftrightarrow \frac{1}{\phi}\frac{d\phi}{du} = \mathcal{J}(u) \tag{27}$$

where $\mathcal{J}$ may be given as an analytic or numeric operator. Equation 27 constructs a relationship between u and ϕ from $h(t)$ over the range of t from τ_1 to $\tau_{\max}$. Integrating $\mathcal{J}(u)$ over the range of data, the relationship between volume fraction ϕ and settling rate u is

$$\log(\phi) - \log(\phi^*) = \int_{u(\phi^*)}^{u} \mathcal{J}(\zeta)d\zeta \tag{28}$$

where $\phi^* = \phi_0$ for mode 3a settling. Thus $f(\phi)$ for settling modes 2a and 3b is

$$f(\phi) = \phi\{\mathcal{H}\}^{-1}\left(\frac{\phi}{\phi^*}\right) \qquad \text{for } \phi^* \le \phi < \phi_{\max} \tag{29}$$

where $\{\mathcal{H}\}^{-1}$ denotes the inverse of the function

$$\mathcal{H}(u) = \exp\left\{\int_{u(\phi^*)}^{u} \mathcal{J}(\zeta)d\zeta\right\} \tag{30}$$

In summary, the $f(\phi)$ information extracted for each mode is

- modes 1, 2a, 3b: $f(\phi_0)$
- mode 2b: $f(\phi)$; $\phi^* \le \phi \le \phi_{\max}$, $f(\phi_0)$ and $f'(\phi^*)$
- mode 3a: $f(\phi)$; $\phi_0 \le \phi \le \phi_{\max}$

A relevant optimization question is which initial concentration generates the most $f(\phi)$ data for a single settling test. Clearly, $\phi_0 = \phi_{\inf}$ (mode 3a) gives the greatest continuous range, but no information is available below $\phi_{\inf}$, which is important if the maximum settling flux is required. Alternately, mode 2b sedimentation for $\phi_0 < \phi_{\inf}$ gives $f(\phi_0)$ below the inflection point, but at the expense of reducing the continuous range above $\phi_{\inf}$. Because the relevant solids concentrations in dewatering applications may vary significantly, the optimum data range varies with application.

The techniques presented above facilitate estimation of $f(\phi)$ from a theoretical $h(t)$ curve. However, $h(t)$ data may be subject to experimental error and are generally given as discrete data. In the following section mechanisms for deviation from the theoretical $h(t)$ curve are considered as well as implications for subsequent analyses.

Considerations of Experimental Systems

In practice, Eq. 1 does not fully capture the dynamics of batch settling at early times, attributed to phenomena such as channel formation and decay of internal flows. These effects are collectively termed "initialization" mechanisms, which act to retard sedimentation, resulting in S-shaped settling curves. The time when these effects become negligible is denoted τ_0.

It is assumed that the initialization mechanisms do not have lasting effects beyond τ_0, and thus do not influence the resulting macroscopic solids distribution, except for a temporal delay in the sedimentation. Consequently, the theoretical settling curve $h(t)$ may be constructed from an observed curve exhibiting initialization dynamics by extrapolation of the linear region. If no linear region is observed, the analysis is problematic because the maximum settling rate $u(\phi_0)$ is not observed and there is no known method to circumvent this problem.

Furthermore, experimental data are sampled as discrete points and may also be subject to experimental error. Standard data smoothing and/or filtering techniques are unsuitable given that $h'(t)$ may be discontinuous, so fitting methods are used to provide continuous functions over the linear and nonlinear regions, and the boundaries τ_0, τ_1 are be estimated simultaneously. A method to fit a continuous curve to observed data is outlined as follows.

To initially smooth the experimental data points (denoted $h_{e,i}$), a median filter over a span of 21 points is used and the series is padded with 10 values of L at the left and 10 values of h_∞ at the right, where h_∞ is the equilibrium bed height. The minimum gradient $\Delta h_{\min}$ over four data points is then calculated

$$\Delta h_{\min} = \min\left\{\frac{h_{e,i+3} - h_{e,i}}{t_{i+3} - t_i}\right\} \tag{31}$$

and the assumption is made that the corresponding time $t_{\Delta h_{\min}}$ lies within the linear region of the settling curve. If the surrounding points do not follow a linear trend, it cannot be established that the settling curve exhibits a linear region. If a linear region is present, $\hat{\tau}_0$ and $\hat{\tau}_1$ are guessed, subject to $\hat{\tau}_0 < t_{\Delta h_{\min}} < \hat{\tau}_1$ and the line $\hat{h}_1(t)$ is fitted to the data over this range. Subsequently, the five-parameter nonlinear function

$$\hat{h}_2(t) = \hat{h}_1(\hat{\tau}_1) + a_0 t^{a_1} - a_0\hat{\tau}_1^{a_1} + a_2^t - a_2^{\hat{\tau}_1} + \frac{a_3}{a_4 + t} - \frac{a_3}{a_4 + \hat{\tau}_1} \tag{32}$$

is fitted to the data for $t > \hat{\tau}_1$, thus ensuring $\hat{h}_2(\hat{\tau}_1) = \hat{h}_1(\hat{\tau}_1)$. Although it is unlikely that a universally applicable functional form exists for data in the range $t > \tau_1$, Eq. 32 appears to be appropriate. A parabolic function $\hat{h}_0(t)$ is used to fit the initialization mechanics for $t < \hat{\tau}_0$, and so the resultant fit $\hat{h}(t)$ is given as the hybrid function

$$\hat{h}(t) = \begin{cases} \hat{h}_0(t) & 0 \le t < \hat{\tau}_0 \\ \hat{h}_1(t) & \hat{\tau}_0 \le t < \hat{\tau}_1 \\ \hat{h}_2(t) & \hat{\tau}_1 \le t \end{cases} \tag{33}$$

The associated root mean square (rms) error is calculated as

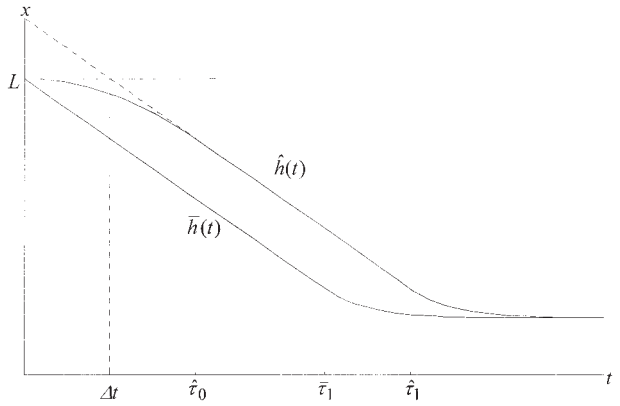

Figure 8. Construction of theoretical settling curve $\bar{h}$(t) from the observed settling curve $\hat{h}$(t).

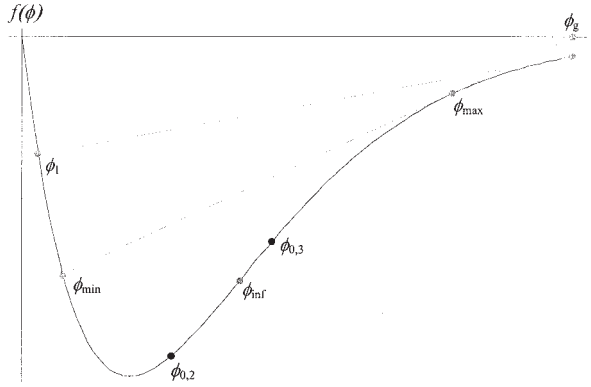

Figure 9. Settling flux curve $f(\phi)$ (Eq. 38) with analytic limits ϕ_{min}, ϕ_{max}, inflection point ϕ_{inf}, mode 1/2 boundary value ϕ_1, and initial concentrations $\phi_{0,2}$, $\phi_{0,3}$.

$$h_{rms} = \sqrt{\frac{\sum_i [h_{e,i} - \hat{h}_n(t_i)]^2}{\sum_i h_{e,i}^2}} \tag{34}$$

and $\hat{\tau}_0$, $\hat{\tau}_1$ iterated until this error is minimized. This process is repeated with the exception that $\hat{h}_2(t)$ is replaced with the four-parameter function

$$\hat{h}_3(t) = \hat{h}_1(\hat{\tau}_1) + a_0 t^{a_1} - a_0 \hat{\tau}_1^{a_1} + a_2^t - a_2^{\hat{\tau}_1} + (\hat{\tau}_1 + a_3) \times \left(1 - \frac{\hat{\tau}_1 + a_3}{t + a_3}\right)[\hat{h}_1'(\hat{\tau}_1) - a_0 a_1 \hat{\tau}_1^{a_1 - 1} - a_2^{\hat{\tau}_1} \log(a_2)] \tag{35}$$

thus ensuring $\hat{h}_3(\hat{\tau}_1) = \hat{h}_1(\hat{\tau}_1)$ and $\hat{h}_3(\hat{\tau}_1) = \hat{h}_1(\hat{\tau}_1)$, that is, $\hat{h}(t)$ is smooth and continuous at $\hat{\tau}_1$. As such, this construction reflects the behavior of mode 3 type settling, whereas $\hat{h}_2(t)$ corresponds to mode 2. If the minimum rms error in this case [using $\hat{h}_3(t)$] is not 10% greater than the mode 2 case [using $\hat{h}_2(t)$], the assumption is made that mode 3 settling is present and so the fit using $\hat{h}_3(t)$ is used. In either case, analysis of the estimated curve $\hat{h}(t)$ is the same.

The estimated theoretical curve $\bar{h}(t)$ (that is, the observed sedimentation curve with initialization dynamics removed) is then constructed as

$$\bar{h}(t) = \begin{cases} \hat{h}_1(t + \Delta t) & 0 \le t < \bar{\tau}_1 \\ \hat{h}_{2,3}(t + \Delta t) & \bar{\tau}_1 \le t \end{cases} \tag{36}$$

where $\bar{\tau}_1 = \hat{\tau}_1 - \Delta t$, and Δt is such that $\hat{h}_1(\Delta t) = L$, as shown in Figure 8. The condition 17 to ensure $\phi_{min} < \phi_0 < \phi_{max}$ is now

$$\frac{\bar{h}(\bar{\tau}_1)}{\bar{\tau}_1} > -\bar{h}'(\bar{\tau}_1) \frac{\phi_0}{\phi_g - \phi_0} \tag{37}$$

Given satisfaction of condition 37 estimation of the flux function $\bar{f}(\phi)$ follows application of the $h(t) \Rightarrow f(\phi)$ transform to $\bar{h}(t)$, as described by Eqs. 26–30. Because the $h(t) \Rightarrow f(\phi)$ transform integrates with increasing ϕ along the $f(\phi)$ curve, estimates $\bar{f}(\phi)$ for $\phi \le \phi_{max}$ are not contaminated by consideration of $\phi > \phi_{max}$. As such, ϕ_{max} can be estimated a posteriori, and the $\bar{f}(\phi)$ [and corresponding $\bar{R}(\phi)$] curve truncated at $\bar{\phi}_{max}$

$$\bar{\phi}_{max} = \phi : \bar{f}'(\phi) = \frac{\bar{f}(\phi)}{\phi - \phi_g} \tag{38}$$

Analysis of Synthetic Data

To test the accuracy of this method for estimation of $R(\phi)$, synthetic $(h_{e,i}, t_i)$ data are analyzed for cases of mode 2b and 3a settling. The test $R(\phi)$ function is

$$R(\phi) = 10^{10}(1 - \phi)^{-20} \tag{39}$$

and if $\Delta\rho = 2500$ kg m^{-3}, the corresponding flux function is

$$f(\phi) = -2.45163 \times 10^{-6} \phi (1 - \phi)^{22} \tag{40}$$

The test suspension gel point is given as $\phi_g = 0.22$, and so $\phi_1 = 0.0065$, $\phi_{min} = 0.0582$, $\phi_{inf} = 0.0870$, and $\phi_{max} = 0.1718$. Two different initial concentrations ($\phi_{0,2} = 0.06$ and $\phi_{0,3} = 0.10$) are considered that are associated with settling modes 2b and 3a, respectively, as illustrated by Figure 9.

An initial height $L = 0.25$ m is used in all cases, and a synthetic $h(t)$ curve is generated from $f(\phi)$ (Eq. 40) by using the inverse $h(t) \Rightarrow f(\phi)$ transform. The quadratic function $L - a_n t^2$ for $0 \le t \le \tau_0$ is used to model the initialization dynamics. At time τ_0, the gradient of this function is equal to $f(\phi_0)/\phi_0$, the linear settling rate of $h(t)$. For $t \ge \tau_0$, the $h(t)$ curve is shifted by Δt, and so the observed settling curve is modeled as

Table 1. Average R_{rms} Error, Standard Deviation (SD), and 90% Confidence Interval for Mode 2b Settling

h_{err} (mm)	N	Average	SD	90% Confidence Interval
2	20	0.0152	0.0867	(−12.6%, 15.7%)
2	50	0.0127	0.0767	(−11.4%, 13.9%)
2	100	0.0089	0.0534	(−7.8%, 9.6%)
5	20	0.0354	0.1064	(−14.1%, 21.1%)
5	50	0.0363	0.1003	(−12.9%, 20.1%)
5	100	0.0351	0.0903	(−11.4%, 18.5%)

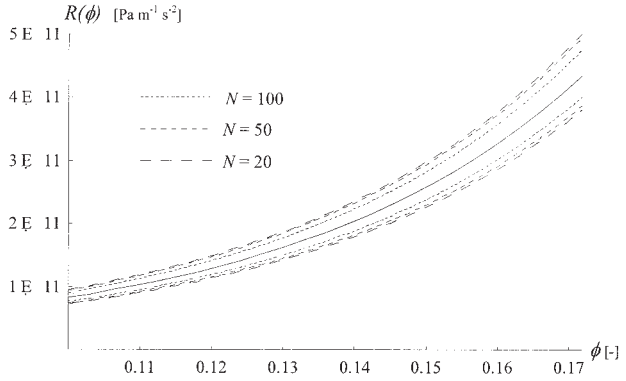

Figure 10. $\bar{R}(\phi)$ estimate 90% confidence intervals for mode 2b settling.

h_{err} = 2.0 mm and N = 20, 50, 100 data points.

$$\hat{h}(t) = \begin{cases} L - a_n t^2 & 0 \le t < \tau_0 \\ h(t + \Delta t) & \tau_0 \le t < \tau_1 + \Delta t \end{cases} \quad (41)$$

The parameter a_n controls the timescale of the initialization mechanics, and the transition time τ_0 is

$$h'(\tau_0) = \frac{f(\phi_0)}{\phi_0} \Rightarrow \tau_0 = \frac{1}{2a_n}\frac{f(\phi_0)}{\phi_0} \quad (42)$$

which results in a shift to the right of the theoretical curve by $\Delta t = \tau_0/2$. The value of a_n used throughout is $a_n = 2 \times 10^{-12}$ m s^{-2}. To construct simulated experimental data ($h_{e,i}$, t_i), the synthetic observed curve $h_n(t)$ is then sampled at frequency ω_s, and Gaussian noise at level h_{err} is added

$$\{h_{e,i}, t_i\} = \left\{ h_n\left[\frac{i}{\omega_s} + h_{err}\text{erf}^{-1}(2X - 1), \frac{i}{\omega_s}\right]\right\} \quad i = 1 \ldots N \quad (43)$$

where X is a uniformly distributed random number in the range [0, 1] and erf^{-1} is the inverse normal error function. The number of synthetic experimental data points is N, where $N = \omega_s(\tau_2 + \Delta t)$. The estimated settling flux $\bar{f}(\phi)$ for each settling mode is then calculated using the curve-fitting method for experimental data and the $h(t) \Rightarrow f(\phi)$ transform. To ascertain the accuracy of the technique, $\bar{R}(\phi)$ is subsequently calculated and the rms error R_{err} is then calculated

$$R_{rms} = \text{sgn}\left[\int_{\phi^*}^{\phi_{\max}} [\bar{R}(\phi) - R(\phi)]d\phi\right]\sqrt{\frac{\int_{\phi^*}^{\phi_{\max}} [\bar{R}(\phi) - R(\phi)]^2 d\phi}{\int_{\phi^*}^{\phi_{\max}} R(\phi)^2 d\phi}} \quad (44)$$

which reflects whether $\bar{R}(\phi)$ is underestimated or overestimated. For each settling mode, 1000 simulations are performed for each combination of N = 20, 50, and 100 points and h_{err} = 2 and 5 mm. In comparison, Pashias (1997) reported that experimental errors less than approximately 0.2 mm are possible, so the errors here are greatly overestimated.

Table 2. Average R_{rms} Error, Standard Deviation (SD), and 90% Confidence Interval for Mode 3a Settling

h_{err} (mm)	N	Average	SD	90% Confidence Interval
2	20	0.0161	0.0492	(−6.4%, 9.6%)
2	50	0.0157	0.0458	(−5.9%, 9.0%)
2	100	0.0156	0.0313	(−3.6%, 6.7%)
5	20	0.0377	0.0881	(−10.6%, 18.1%)
5	50	0.0090	0.0613	(−9.1%, 10.9%)
5	100	0.0046	0.0517	(−8.0%, 8.9%)

The resultant average, standard deviation (SD), and 90% confidence interval of the R_{rms} errors for mode 2b settling are summarized in Table 1. The 90% confidence intervals and the test $R(\phi)$ curve (Eq. 39) for h_{err} = 2 and 5 mm are illustrated in Figures 10 and 11, respectively. As expected, the accuracy of the estimates increases with increasing N and decreasing h_{err}. For h_{err} = 2 mm, the influence of the number of data points is significant. Because $h'(t)$ is discontinuous at τ_1 for mode 2b settling, errors associated with estimation of $h'(\tau_1^+)$ influence ϕ^* (see Eq. 20), and so a high density of measurements around τ_1 is desirable. The influence of N for h_{err} = 5 mm is not as significant because of the level of noise masking the discontinuity in $h'(t)$ at τ_1.

Given minimization of experimental error and maximization of measurements, accurate estimates of $R(\phi)$ are possible for

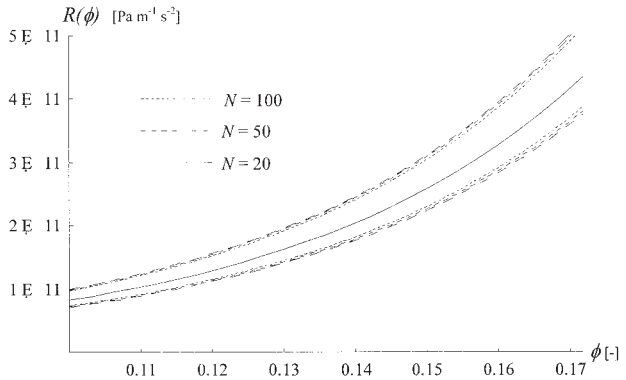

Figure 11. $\bar{R}(\phi)$ estimate 90% confidence intervals for mode 2b settling.

h_{err} = 5.0 mm and N = 20, 50, 100 data points.

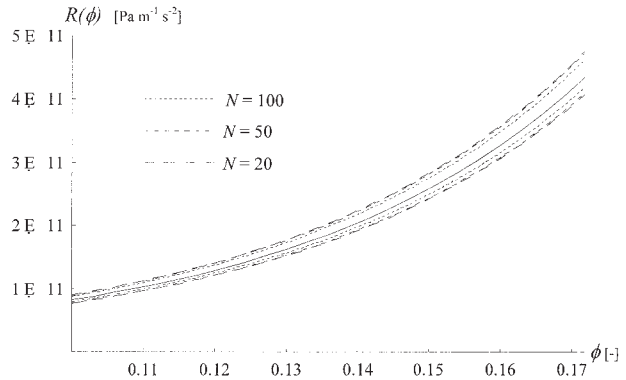

Figure 12. $\bar{R}(\phi)$ estimate 90% confidence intervals for mode 3 settling.

h_{err} = 2.0 mm and N = 20, 50, 100 data points.

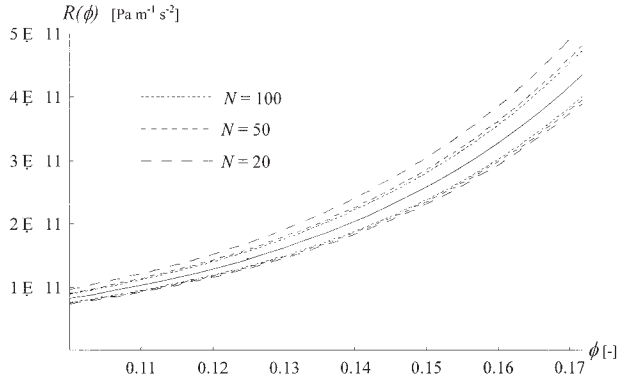

Figure 13. $\bar{R}(\phi)$ estimate 90% confidence intervals for mode 3 settling.

h_{err} = 5.0 mm and N = 20, 50, 100 data points.

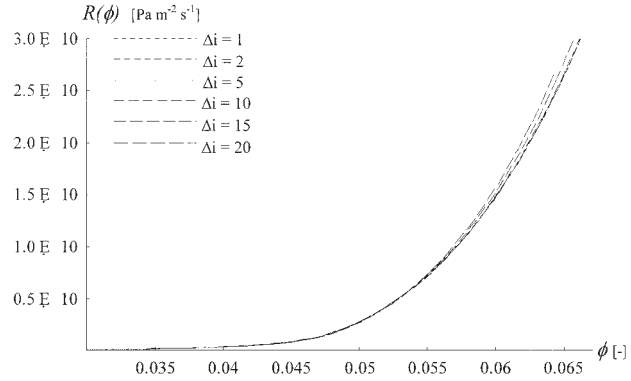

Figure 15. $\bar{R}(\phi)$ estimates from L = 0.36 m data for Δi = 1, 2, 5, 10, 20.

mode 2b settling. The incorrect mode of settling was inferred in about 2% of cases, and in such cases the R_{rms} errors are high. Consistent overestimation of $R(\phi)$ suggests that the gradient $h'(\tau_1^+)$ is underestimated as a result of the diffusive effect of the random noise at τ_1. Accurate estimation of this gradient is critical to the success of mode 2b settling analysis, although a clear discontinuity in $h'(t)$ is seldom observed for experimental systems.

Mode 3a sedimentation represents a simpler case to analyze than mode 2b because $h'(t)$ is continuous throughout. This restriction removes one degree of freedom from the curve fit, and avoids errors associated with estimation of $h'(\tau_1^+)$. However, because the boundary τ_1 is less pronounced in this case, errors associated with estimation of τ_1 are greater. Furthermore, the technique must identify the correct settling mode from the simulated experimental data alone.

Significant errors can arise if mode 2b settling is inferred, the probability of which is low, but does increase with increasing h_{err} and decreasing N. The R_{rms} statistics for h_{err} = 2 and 5 mm and N = 20, 50, and 100 points are summarized in Table 2, and the 90% confidence intervals for h_{err} = 2 and 5 mm are illustrated in Figures 12 and 13, respectively.

Quite accurate estimates for h_{err} = 2 mm are possible, especially if a large number of sample points are used. For h_{err} = 5 mm, these errors are increased somewhat, although reasonable estimates are possible if $N \geq 50$. The tendency to overestimate $R(\phi)$ may be attributed to the linear region of $h(t)$ not being faithfully represented by the discrete data points, especially for N = 20. In such cases, the maximum settling rate may not be expressed, and thus is overestimated, and this error is amplified with integration along the $h(t)$ curve. In general, the estimates of $\bar{R}(\phi_0)$ are more accurate for mode 3a settling, with respect to the issues outlined above. Mode 3a also generally generates estimates of $R(\phi)$ over a greater range of ϕ.

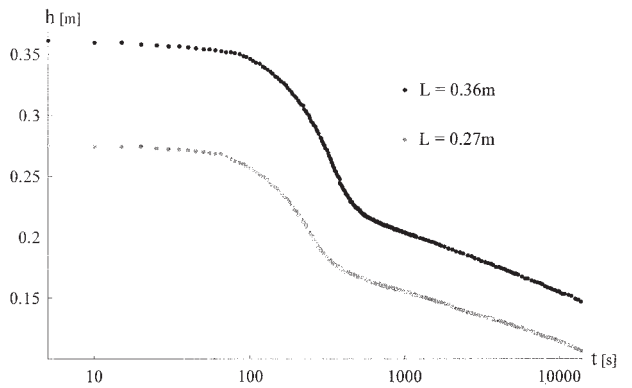

Figure 14. Hematite $h(t)$ settling data for L values of 0.36 and 0.27 m.

Analysis of Experimental Data

From the analysis of synthetic data, accurate estimates of $R(\phi)$ may be obtained, given a significant number of measurements and good experimental technique. It is also desirable to test the method for experimental data, although in this case, the actual $R(\phi)$ function is unknown. As such, two independent batch-settling experiments are analyzed, and the accuracy of the method is determined by the correlation between the predicted hindered settling functions. A hematite suspension at solids concentration ϕ = 0.03 was coagulated using 2.0 M NaOH, which was subsequently sonicated and placed on an orbital shaker for 12 h. The suspension was then decanted up to a height of 36 cm in a measuring cylinder, and the resultant $h(t)$ profile measured until equilibrium. This process was repeated for an initial height of 27 cm. A log-linear plot of the settling data is illustrated in Figure 14, which shows both experiments to be examples of mode 3 settling.

To maximize accuracy, 231 data points are measured in each case, which represents an upper limit of N for manual measurement. To simulate more common experiments, this data set is reduced such that every Δith point is used in the analysis. For L = 0.36 m, $\bar{R}(\phi_0)$ is estimated for Δi = 1, 2, 5, 10, 15, and 20. The estimates are illustrated in Figure 15, which show very good agreement for all values of Δi. It is noted that the major effect of increasing Δi (or decreasing N) is to reduce the range of predicted ϕ, rather than the accuracy of the estimates $\bar{R}(\phi_0)$.

Table 3. R_{rms} Error for L = 0.36 m, Δi = 2, 5, 10, 15, 20

Δi	R_{rms}
2	0.0015
5	0.0253
10	0.0191
15	0.0591
20	0.0556

The rms error for Δi, in comparison to the case of $\Delta i = 1$, is calculated as

$$R_{rms} = \mathrm{sgn}\left[\int_{\phi_0}^{\tilde{\phi}_{\max}} [\bar{R}_{\Delta i}(\phi) - \bar{R}_{\Delta i=1}(\phi)]d\phi\right] \times \sqrt{\frac{\int_{\phi_0}^{\tilde{\phi}_{\max}} [\bar{R}_{\Delta i}(\phi) - \bar{R}_{\Delta i=1}(\phi)]^2 d\phi}{\int_{\phi_0}^{\tilde{\phi}_{\max}} \bar{R}_{\Delta i=1}(\phi)^2 d\phi}} \quad (45)$$

where $\tilde{\phi}_{\max}$ is the minimum value of $\phi_{\max}$ between $\bar{R}_{\Delta i}(\phi)$ and $\bar{R}_{\Delta i=1}(\phi)$. The rms errors for $\Delta i = 2 \rightarrow 20$ are summarized in Table 3, which reflect the consistency in predictions of $\bar{R}_{\Delta i}(\phi)$. Again as N is decreased, the tendency to overestimate $R(\phi)$ increases. Although not shown here, similar results were obtained for the case of $L = 0.27$ m.

To compare the independent experiments, $\bar{R}(\phi)$ was estimated for the cases $L = 0.36$ m ($\Delta i = 1$) and $L = 0.27$ m ($\Delta i = 1$). These results are illustrated in Figure 16 and show good agreement with the predictions. It is noted that the suspensions were synthesized independently, and thus the material properties may not be identical.

By assuming the predicted $\bar{R}(\phi)$ for $L = 0.36$ m ($\Delta i = 1$) to be the actual $R(\phi)$ for the suspension, the rms errors for $L = 0.27$ m are calculated in a similar fashion to Eq. 45. These results are presented in Table 4, which also show a slight decrease in accuracy with increasing Δi. Although these results suggest $N \cong 20$ is capable of producing accurate estimates of $R(\phi)$, it is recommended that $N > 50$ be used to ensure accuracy of the fit, and multiple tests are advisable to establish consistency.

Conclusions

By using the entropy condition, unique analytic solutions of batch-settling experiments for $\phi < \phi_g$ are possible. Consequently, the hindered settling function for $R(\phi)$ for $\phi < \phi_{\max}$ may be predicted from the dynamics of sediment/supernatant interface $h(t)$ alone. The techniques presented here are capable of addressing the issues associated with experimental data, provided a linear region is observed in the $h(t)$ profile. The advantage of this method is that no information is required regarding the suspension a priori, aside from ϕ_0, ϕ_g, and $\Delta\rho$.

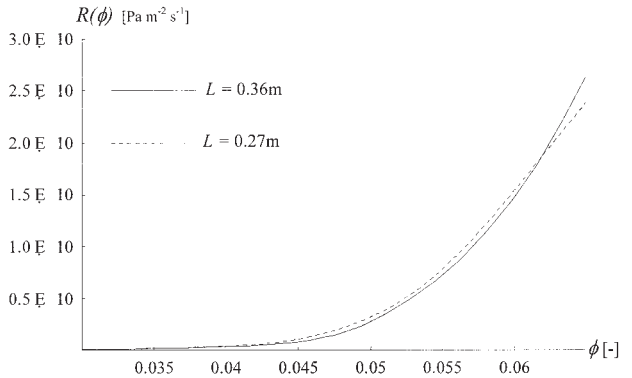

Figure 16. Comparison of $\bar{R}(\phi)$ estimates from $L = 0.36$, 0.27 m data for $\Delta i = 1$.

Table 4. R_{rms} Error for $L = 0.27$ m, $\Delta i = 2, 5, 10, 15, 20$

Δi	R_{rms}
1	0.0571
2	0.0584
5	0.0575
10	0.0587
15	0.0464
20	0.0604

From the accuracy of the synthetic analysis and consistency of the experimental analysis, it appears $R(\phi)$ can reliably be estimated with precision from batch-settling data. For the cases assessed, analysis of mode 2b settling is less accurate than mode 3a. In all cases, it is recommended that a high data sampling frequency be used around the linear region of $h(t)$ to determine the boundaries τ_0, τ_1 with accuracy. Estimation of these boundaries appears to be the major source of error in $\bar{R}(\phi)$. Because batch-settling experiments are simple and cheap to perform, the methods presented here facilitate characterization of unnetworked suspensions both on site and in the laboratory.

To estimate $R(\phi)$ for $\phi \geq \phi_g$, knowledge of the compressibility $P_y(\phi)$ is required. Furthermore, analytic solution is not possible and thus the associated inverse problem must be solved numerically. Despite these hurdles, sufficient scope now exists for characterization of suspensions from batch-settling data alone. In conjunction with pressure filtration data, complete characterization over all relevant ϕ data is possible.

Acknowledgments

The authors thank D. Hill for the experimental hematite settling data and the support of an Australian Postgraduate Award (Industry) is acknowledged. Financial support was through the Particulate Fluids Processing Centre, a Special Research Centre of the Australian Research Council.

Notation

$a_0 \cdots a_4$ = $h(t)$ fitting parameters
a_n = initialization mechanics parameter, m s^{-2}
$D(\phi)$ = the solids diffusion function accounting for sediment compressibility, m^2 s^{-1}
erf^{-1} = inverse error function
D/Dt = material derivative, s^{-1}
$\underline{f}(\phi)$ = settling flux, m s^{-1}
$f(\phi)$ = estimated settling flux, m s^{-1}
g = gravitational acceleration, m s^{-2}
$h(t)$ = theoretical sediment/supernatant interface height, m
$h_{0(t)} \cdots h_{3(t)}$ = components of $h(t)$, m
$\hat{h}(t)$ = observed interface height, m
$\bar{h}(t)$ = estimated theoretical settling curve, m
h_∞ = equilibrium interface height datum, m
$\mathcal{J}$ = $h(t) \Rightarrow f(\phi)$ transform operator
$\mathcal{H}$ = $h(t) \Rightarrow f(\phi)$ transform operator
L = initial suspension height, m
p_N = network pressure, Pa
$P_{y(\phi)}$ = compressive yield stress, Pa
$R(\phi)$ = hindered settling function, Pa m^{-1} s^{-2}
$\bar{R}(\phi)$ = estimated hindered settling function, Pa m^{-1} s^{-2}
R_{rms} = rms error in $\bar{R}(\phi)$
t = time coordinate, s
$u(\phi)$ = settling velocity, m s^{-1}
sgn = sign function
x = vertical coordinate
x_b = consolidating bed position, m
x_c = characteristic position, m
x_{cd} = contact discontinuity position, m

x_s = shock position, m
X = uniformly distributed random number

Greek letters

$\Delta\rho$ = interphase density difference
Δh_{min} = minimum interface height gradient, m s^{-1}
Δi = data filtering parameter
Δt = time shift associated with initialization mechanics, s
σ = shock propagation velocity, m s^{-1}
ξ = $h(t) \Rightarrow f(\phi)$ transform operator
τ_0 = time associated with decay of initialization mechanics, s
τ_1 = onset time of nonlinearity in $h(t)$, s
τ_2 = time at which only consolidating bed and supernatant remain, s
τ_{max} = time associated with onset of nonlinearity in $h(t)$, s
ϕ = solids volume fraction
ϕ_g = suspension gel point
ϕ_0 = initial solids volume fraction
ϕ_1 = mode 1/2 boundary solids volume fraction
ϕ_{min} = minimum analytic solids volume fraction
ϕ_{max} = maximum analytic solids volume fraction
ϕ_{inf} = inflection point for $f(\phi)$
$\tilde{\phi}_{max}$ = maximum expressed ϕ
ϕ^* = solids concentration at $h(\tau_1^+)$
ω_s = sampling frequency, s^{-1}

Subscripts and superscripts

+, − = upper, lower discontinuity limit values

Literature Cited

Auzerais, F. M., R. Jackson, and W. B. Russel, "The Resolution of Shocks and the Effects of Compressible Sediments in Transient Settling," *J. Fluid Mech.*, **195**, 437 (1988).

Bürger, R., and F. Concha, "Mathematical Model and Numerical Simulation of the Settling of Flocculated Suspensions," *Int. J. Multiphase Flow*, **24**(6), 1005 (1998).

Bürger, R., and E. M. Tory, "On Upper Rarefaction Waves in Batch Settling," *Powder Technol.*, **108**(1), 74 (2000).

Bürger, R., and W. L. Wedland, "Entropy Boundary and Jump Conditions in the Theory of Sedimentation with Compression," *Math. Methods Appl. Sci.*, **21**(9), 865 (1998).

Buscall, R., and L. R. White, "The Consolidation of Concentrated Suspensions," *J. Chem. Soc. Faraday Trans. 1*, **83**(3), 873 (1987).

Bustos, M. C., F. Concha, R. Bürger, and E. M. Tory, *Sedimentation and Thickening: Phenomenological Foundation and Mathematical Theory*, Kluwer Academic, Dordrecht, The Netherlands (1999).

Cheng, K. S., "Asymptotic Behavior of Solutions of a Conservation Law without Convexivity Conditions," *J. Differ. Equations*, **40**, 343 (1981).

Cheng, K. S., "A Regularity Theorem for a Nonconvex Scalar Conservation Law," *J. Differ. Equations*, **61**, 79 (1986).

de Kretser, R. G., S. P. Usher, P. J. Scales, D. V. Boger, and K. A. Landman, "Rapid Filtration Measurement of Dewatering Design and Optimization Parameters," *AIChE J.*, **47**(8), 1758 (2001).

Diplas, P., and A. N. Papanicolaou, "Batch Analysis of Slurries in Zone Settling Regime," *J. Environ. Eng.*, **123**(7), 659 (1997).

França, S. C. A., G. Massarani, and E. C. Biscaia, Jr., "Study on Batch Sedimentation Simulation—Establishment of Constitutive Equations," *Powder Technol.*, **101**(2), 157 (1999).

Green, M. D., *Characterisation of Suspensions in Settling and Compression*, PhD Thesis, Dept. of Chemical Engineering, The University of Melbourne, Melbourne, Australia, p. 246 (1997).

Green, M. D., M. Eberl, and K. A. Landman, "Compressive Yield Stress of Flocculated Suspensions: Determination via Experiment," *AIChE J.*, **42**(8), 2308 (1996).

Howells, I., K. A. Landman, A. Panjkov, C. Sirakoff, and L. R. White, "Time Dependent Batch Settling of Flocculated Suspensions," *Appl. Math. Model.*, **14**, 77 (1990).

Kynch, G. J., "A Theory of Sedimentation," *Trans. Faraday Soc.*, **48**, 166 (1952).

Landman, K. A., and W. B. Russel, "Filtration at Large Pressures for Strongly Flocculated Suspensions," *Phys. Fluids A*, **5**(3), 550 (1993).

Landman, K. A., C. Sirakoff, and L. R. White, "Dewatering of Flocculated Suspensions by Pressure Filtration," *Phys. Fluids A*, **3**(6), 1495 (1991).

Landman, K. A., J. M. Stankovich, and L. R. White, "The Measurement of Filtration Diffusivity $D(\phi)$ of a Flocculated Suspension," *AIChE J.*, **45**(9), 1875 (1999).

Landman, K. A., and L. R. White, "Determination of the Hindered Settling Factor for Flocculated Suspensions," *AIChE J.*, **38**(2), 184 (1992).

Landman, K. A., and L. R. White, "Solid/Liquid Separation of Flocculated Suspensions," *Adv. Colloid Interface Sci.*, **51**, 175 (1994).

Oleinik, O. A., "Discontinuous Solutions of Nonlinear Differential Equations," *Am. Math. Soc. Transl. Ser. 2*, **26**, 95 (1963).

Pashias, N., *The Characterisation of Bauxite Residue Suspensions in Shear and Compression*, PhD Thesis, Dept. of Chemical Engineering, The University of Melbourne, Melbourne, Australia, p. 312 (1997).

Prilepko, A. I., D. G. Orlovsky, and I. A. Vasin, *Methods for Solving Inverse Problems in Mathematical Physics*, Marcel Dekker, New York, NY (2000).

Tiller, F. M., and Z. Khatib, "The Theory of Sediment Volumes of Compressible, Particulate Structures," *J. Colloid Interface Sci.*, **100**(1), 55 (1984).

Tiller, F. M., and M. Shirato, "The Role of Porosity in Filtration: VI. New Definition of Filtration Resistance," *AIChE J.*, **10**(1), 61 (1964).

Usher, S. P., R. G. de Kretser, and P. J. Scales, "Validation of a New Filtration Technique for Dewaterability Characterization," *AIChE J.*, **47**(7), 1561 (2001).

Manuscript received Sept. 2, 2003, revision received Jun. 2, 2004, and final revision received Dec. 6, 2004.